Journal of Electronic Materials (2022) 51:6995–7008
https://doi.org/10.1007/s11664-022-09929-5

ORIGINAL RESEARCH ARTICLE

The Impact of the Presence of Aromatic Rings in the Substituent on the Performance of C_{60}/C_{70} Fullerene-Based Acceptor Materials in Photovoltaic Cells

Wojciech Mech[1] · Piotr Piotrowski[2] · Kamila Zarębska[2] · Krzysztof P. Korona[1] · Maria Kaminska[1] · Magdalena Skompska[2] · Andrzej Kaim[2]

Received: 23 June 2022 / Accepted: 30 August 2022 / Published online: 25 September 2022

Abstract

In this work, a series of C_{60}/C_{70} fullerene derivatives bearing non-aromatic and mono-, bi-, tri- and tetracyclic aryl-substituents was synthesized according to the modified Bingel method and characterized using spectral methods: ESI-MS, ^{1}H NMR, ^{13}C NMR, UV–Vis, FT-IR and cyclic voltammetry (CV). HOMO and LUMO energy levels and the band gaps for optimized structures of reported fullerene derivatives were determined according to the DFT functionals, B3LYP 6-31G(d) and PBE/6-311G(d,p). Results obtained from CV and UV–Vis measurements, which showed very good agreement, were compared to calculated theoretical values also revealing satisfactory level of compliance of the obtained results. We have studied the impact of presence and number of aromatic rings in malonate substituent of C_{60}/C_{70} fullerene derivatives employed as acceptor materials on performance of BHJ solar cells prepared using PTB7-Th as donor material. We successfully prepared solar cells based on all the synthesized compounds, and the highest performance of the obtained photovoltaic devices was observed for fullerene derivatives bearing monocyclic and bicyclic aromatic moieties. The obtained voltage was about 0.8 V and current density was above 10 mA/cm^2. Optical studies showed absorption edges at 1.9 eV and 1.8 eV for C_{60} and C_{70} derivatives, respectively, with absorption coefficients comparable to C_{60}/C_{70} PCBM samples. Photocurrent spectroscopy showed 20–40% quantum efficiency. Long-term ageing measurements showed T80 time between 105 days and 115 days for derivatives with phenyl and naphthalene substituents. Taking into account that synthesis of reported fullerene derivatives is very convenient, the reported compounds are very promising materials for construction of BHJ solar cells.

Keywords Fullerenes · photovoltaics · solar cells

Introduction

The rise of organic photovoltaics (OPV) serving as a renewable energy source, has become one of the most important directions of current scientific research.[1,2] It is hard to mention all improvements reported since fabrication of the first bulk heterojunction solar cell.[3,4] Efforts by scientists have led to materials with parameters that allow them to be used in commercial devices.[5]

However, development of suitable active layer materials, which is essential to achieve high-performance of the constructed device, is still a challenging task. Recent years have provided a lot of interesting donor materials, which are readily available.[6,7] On the other hand, the assortment of acceptor materials is not that broad, and despite numerous reports on non-fullerene acceptors,[8] fullerene-based materials remain promising candidates for this purpose.[9–11]

To design and synthesize derivatives with tailored properties, we need to determine the influence of the structure of the fullerene derivative on the performance of the resulting device.[12,13] It is well known that addition of multiple addends results in reduced π-conjugation and also affects the crystal structure of the formed active layer, influencing both charge separation and mobility of the carriers.[14]

Wojciech Mech and Piotr Piotrowski have contributed equally to this work

✉ Piotr Piotrowski
ppiotrowski@chem.uw.edu.pl

[1] Faculty of Physics, University of Warsaw, Pasteura 5, 02-093 Warsaw, Poland

[2] Faculty of Chemistry, University of Warsaw, Pasteura 1, 02-093 Warsaw, Poland

Another important factor is the size and shape of fullerene core that is used as a substrate for synthesis of acceptor materials. In most examples, C_{70} analogues show advantageous properties when comparing to corresponding C_{60} derivatives. Superior performance of C_{70} fullerene-based acceptors is associated mainly with its higher absorption in the visible range, better electron accepting capability and higher photocarrier generation efficiency.[15,16] However, due to the tendency of C_{70} to form bigger aggregates, which can lower the donor–acceptor contact area, in some cases, the C_{60} analogue of the corresponding C_{70} fullerene derivative might lead to higher performance of the resulting solar cell.[17] An alternative path does not use pure C_{60} or C_{70} fullerene derivative but a mixture of identically functionalized C_{60} and C_{70} fullerenes.[18] This approach allows us, in some cases, to obtain an advantageous morphology of formed layers when comparing to pure C_{60}/C_{70} derivatives and achieve saturation of absorption, while allowing the use of a mixture of both fullerenes obtained directly from extraction of fullerene soot, thus avoiding steps associated with purification of each fullerene.

Taking into account the interesting properties of C_{70} fullerene-based acceptor materials, higher fullerenes were also employed for synthesis of acceptor materials for photovoltaic cells. However, the resulting performance of the devices was significantly lower,[19] which combined with low abundance, poor solubility and high cost makes them poorly studied in the field of OPVs.

Similarly, the structure of substituents introduced to the fullerene core, especially the number of aromatic rings, is another factor that can result in heterogeneous performance of engineered OPV devices, as previously shown by Kim et al.[20] However, literature data published on this subject is still inconclusive as to the most appropriate method for functionalization of fullerenes for use as acceptor materials.

In this contribution, we have synthesized a group of new C_{60} and C_{70} derivatives by systematically growing a number of aromatic rings covalently attached to the fullerene core via a malonate linker. All synthesized products were characterized using spectroscopic techniques: ESI–MS, $^{1}H/^{13}C$ NMR and FT-IR.

The aim of the presented research was to investigate the influence of the number of aromatic rings connected to the fullerene core on the properties of synthesized acceptor materials, especially the efficiency of constructed solar cells.

The investigated solar cells had popular bulk heterojunction (BHJ) architecture, and the active layer comprised a mixture of donor and acceptor materials.[21] The active layers contained fullerene derivatives as acceptor materials and PTB7-Th was applied as donor material. We expected that the synthesized C_{60} and C_{70} fullerene derivatives would efficiently absorb light, their electronic levels should match the donor levels, and they should form a composite donor-fullerene structure of appropriate morphology. The use of fullerene derivatives with a different number of aromatic rings in their substituents should allow determination of their optimal number and impact on the morphology of the photosensitive layer, bearing in mind that the morphology and structure of the BHJ can be improved by appropriate active layer processing,[21] addition of some compounds to the layer[22] or engineering of fullerene derivatives.[23]

We have also investigated ageing processes in devices containing different fullerene derivatives. Degradation of polymer-fullerene solar cells has many causes, including degradation of both ITO and metal electrodes, and electron- and hole-blocking layers, but the main degradation process takes place in the active layer, that is, in the donor:acceptor bulk heterojunction. Most of the research indicates that the polymer is sensitive to air-related oxidation[24] and photo-oxidation.[25] The fullerene derivatives are stable but probably can influence reactions occurring in the polymer.

Experimental Section

Reagents

Methylene chloride, *n*-hexane, *n*-pentane and toluene were purchased from POCh (Poland). Fullerenes C_{60} and C_{70} were isolated using preparative HPLC with a 5PBB column from fullerene soot extract bought from MST Nano. Benzophenone, benzyl alcohol, carbon disulphide, carbon tetrachloride suitable for IR spectroscopy, chlorobenzene, 1,8-diiodooctane, deuterated chloroform, 1,8-diazabicycloundec-7-ene, diethyl bromomalonate, ethyl malonyl chloride, iodine, 1-naphthalenemethanol and 9-phenanthrenecarboxaldehyde, 1-pyrenemethanol, potassium bromide FT-IR grade and sodium were bought from Sigma-Aldrich. PC60BM, PC70BM, PTB7-Th and PEDOT:PSS Al4083 water solution were purchased from Ossila. Toluene was dried and purified before use according to standard procedures, and other solvents were analytical-grade reagents and were used as received.

Characterization Methods and Instrumentation

ESI–MS spectra were acquired on a Micromass LCT ESI-TOF mass spectrometer equipped with an orthogonal electrospray ionization source.

^{1}H and ^{13}C NMR spectra were acquired on a Varian Unity Plus 500 MHz spectrometer using $CDCl_3$ a solvent.

The infrared experiments were carried out using a Shimadzu FT-IR-8400S for samples prepared as a KBr disk or as solution in CCl_4.

Cyclic voltammetry (CV) experiments were performed using an Autolab PGSTAT204 potentiostat. A glassy carbon

electrode of 3 mm diameter was used as the working electrode, silver/silver chloride (Ag/AgCl) as the reference electrode and platinum as the counter electrode. The electrochemical experiments were performed using an Autolab PGSTAT302N potentiostat in a three-electrode cell with a Pt disc working electrode with a surface area of 0.03 cm^2, a Pt mesh as the counter electrode and Ag/Ag^+ (0.1 M $AgNO_3$ in CH_3CN) as a double-junction reference electrode, with 0.1 M $TBAPF_6$ in DCM as the filling solution. The potential of Ag/Ag^+ was calibrated using a ferrocene/ferrocenium (Fc/Fc^+) redox couple. Ferrocene was added to the solutions after the measurements as an internal reference. The value of the formal potential ($E^{o\prime}$) for Fc/Fc^+ measured vs. Ag/Ag^+ was 0.05 V. Since $E^{o\prime}$ for the Fc/Fc^+ redox couple in DCM solution is 0.7 V vs. NHE (normal hydrogen electrode),[26] the potential of Ag/Ag^+ (0.1 M, AN) reference electrode used in this work was 0.65 V vs. NHE.

The fullerene derivatives were dissolved in dichloromethane containing 0.1 M $TBAPF_6$ supporting electrolyte. All the solutions before experiments were deoxygenated by bubbling with a stream of Ar for 10 min. The Pt working electrode before each experiment was polished with a polycrystalline diamond suspension (3 µm) (MetaDiTM Supreme, Buehler) on the polishing cloth.

The absorption spectra of the fullerene derivatives in dichloromethane were recorded using a UV–Vis spectrometer Lambda 12 (Perkin-Elmer) in the wavelength range 800–220 nm.

Optical absorbance of thin organic layers on glass substrates was measured by a Metash UV6000 spectrometer and UV-analyst software in a 200–1100 nm (1.2–6.2 eV) range with a 2-nm step.

Optical microscopy images of solar cells were obtained by a Nikon ECLIPSE ME600 microscope with differential interference (Nomarski) contrast and a DeltaPix 5MP digital camera.

Current–voltage characteristics were measured by a Keithley 2450 Source Meter with Kickstart PC software and using an Ossila 8-pixel test board. A Newport VeraSol-2 LED Class AAA Solar Simulator was applied as a source of illumination with a power of 1000 W/m^2 and AM1.5G spectrum. The average power conversion efficiency (PCE) was calculated for eight pixels of each cell.

Photocurrent spectroscopy was performed in the range from 0.3 µm to 1.7 µm (0.7 eV to 4 eV) using the light of a tungsten lamp passing through the monochromator. The current was measured in short-circuit mode (I_{SC}) with a Keithley 26,000 picoammeter. For external quantum efficiency (EQE) calculation, the light intensity spectrum was measured with a PM320E power meter at each wavelength.

The calculations were performed using the Gaussian 16 Revision A.03, software.[27] The optimized structures of the investigated fullerene derivatives with all positive vibration frequencies in vacuum were obtained at the hybrid density functional DFT/B3LYP level with the 6-31G(d) basis set.[28–30] The highest occupied molecular orbital (HOMO) and lowest unoccupied molecular orbital (LUMO) energy levels were estimated on fully optimized structures by employing both DFT/B3LYP 6-31G(d) and PBE/6-311G(d,p)[31] and compared with the cyclic voltammetry experimental values. To calculate the excitation energy of the first excited states, the time-dependent density functional theory (TDDFT) TD-B3LYP/6-31G(d) was employed. The results were then compared with the wavelengths of the UV absorption spectra of the fullerene acceptor derivatives.

Synthesis of Malonate Substrates

The synthesized malonate derivatives are shown in Fig. 1. Benzyl ethyl malonate (**MPh**), was synthesized according to a procedure reported by Gutman et al.[32] Synthesis and characterization of ethyl (pyren-1-ylmethyl) malonate (**MP**) was reported elsewhere.[23,33] Other desired malonic acid esters were obtained using a modified synthesis method reported by de la Torre et al.[34] Briefly, a solution of ethyl malonyl chloride (904 mg, 768 µl, 6 mmol) in anhydrous dichloromethane (30 ml) was added dropwise for a period of 20 min to a well-stirred solution of corresponding alcohol (5 mmol) and triethylamine (668 mg, 920 µl, 6.6 mmol) in dry methylene chloride (70 ml) at 0°C. The reaction mixture was then allowed to warm to room temperature and stirred for additional 16 h. The obtained mixture was concentrated under reduced pressure and afterwards chromatographed on silica gel using 1:2 v/v ethyl acetate/*n*-hexane mixture as an eluent to yield the desired malonate esters.

Phenanthren-9-ylmethanol required for synthesis of ethyl (phenanthren-9-ylmethyl) malonate was synthesized by reduction of 9-phenanthrenecarboxaldehyde using sodium borohydride as described by Fujino et al.[35]

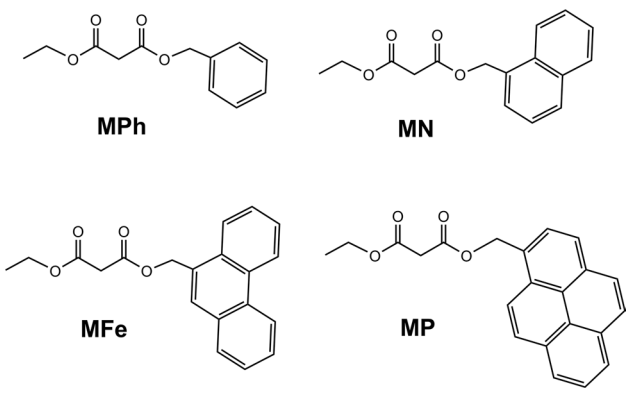

Fig. 1 Structures of synthesized malonate derivatives.

Ethyl(naphtalen-1-ylmethyl) malonate (MN) Yield: 93%; ESI–MS: 295.1 $[M+Na]^+$; ^{1}H NMR (500 MHz, $CDCl_3$) δ 8.01–7.43 (*m*, 7H), 5.64 (*s*, 2H), 4.13 (*q*, $J=7.1$ Hz, 2H), 3.41 (*s*, 2H), 1.17 (*t*, $J=7.2$ Hz, 3H) ppm; ^{13}C NMR (125 MHz, $CDCl_3$) δ 166.52, 166.38, 133.70, 131.58, 130.87, 130.75, 129.53, 128.79, 128.71, 127.76, 126.62, 126.00, 125.23, 123.50, 65.58, 61.56, 41.64, 13.92 ppm; FT-IR (CCl_4) V_{max} (cm^{-1}) 3051.19, 2982.92, 2959.41, 2937.40, 2901.84, 2869.67, 1756.69, 1739.41, 1513.64, 1465.09, 1411.53, 1368.90, 1327.28, 1266.28, 1170.09, 1146.52, 1034.52, 993.48; (Figures S1–S4, Supplementary Material).

Ethyl (phenanthren-9-ylmethyl) malonate (MFe) Yield: 84%; ESI–MS: 345.1 $[M+Na]^+$; ^{1}H NMR (500 MHz, $CDCl_3$) δ 8.77–8.71 (*m*, 4H), 8.67 (d, $J=8.3$ Hz, 4H), 8.05 (dd, $J=8.1$, 1.3 Hz, 4H), 7.92–7.87 (*m*, 4H), 7.84 (*s*, 4H), 7.74–7.58 (*m*, 16H), 7.26 (*s*, 1H), 5.69 (*s*, 8H), 4.15 (*q*, $J=7.1$ Hz, 8H), 3.46 (*s*, 8H), 1.29 (*t*, $J=7.1$ Hz, 7H), 1.19 (d, $J=7.2$ Hz, 12H), ^{13}C NMR (126 MHz, $CDCl_3$) δ 166.08, 130.60, 130.27, 130.23, 129.73, 128.67, 128.43, 128.41, 126.85, 126.51, 126.43, 126.25, 123.76, 122.74, 122.07, 65.54, 61.12, 41.22, 13.47 ppm; FT-IR (KBr) V_{max} (cm^{-1}) 3080.5, 2983.1, 2961.8, 2937.0, 2906.9, 2871.5, 1757.1, 1451.9, 1371.8, 1327.6, 1267.9, 1240.6, 1148.1, 1036.2, 987.5, 887.3; (Figures S5-S8, Supplementary Material).

Synthesis of C_{60}/C_{70} Fullerene Derivatives

61-Bis(ethyloxycarbonyl)-1,2-methano[60]fullerene (**C_{60}-MEB**) and 71-bis(ethyloxycarbonyl)-1,2-methano[70] fullerene (**C_{70}-MEB**) (see Fig. 2) were synthesized using a method reported by Cheng et al.[36]

61-Bis(ethyloxycarbonyl)-1,2-methano[60]fullerene (C_{60}-MEB) Yield: 57%, ESI–MS 901.8 $[M+Na]^+$; ^{1}H NMR (500 MHz, $CDCl_3$) δ 4.54 (*q*, $J=7.1$ Hz, 2H), 1.49 (*t*, $J=7.1$ Hz, 5H); ^{13}C NMR (125 MHz, $CDCl_3$) δ 163.04, 145.19, 145.14, 145.05, 144.74, 144.56, 144.50, 143.77, 142.99, 142.90, 142.88, 142.11, 141.76, 140.84, 138.94, 63.19, 14.23; FT-IR (KBr) V_{max} (cm^{-1}) 1743.1, 1512.2, 1460.0, 1427.9, 1363.9, 1292.8, 1265.3, 1232.3, 1205.8, 1181.7, 1094.4, 1058.8, 1019.2, 860.2, 737.0, 702.7, 670.1, 577.4, 560.8, 551.3, 525.5; (Figures S9–S12, Supplementary Material).

71-Bis(ethyloxycarbonyl)-1,2-methano[70]fullerene (C_{70}-MEB) Yield: 45%, ESI–MS 1021.9 $[M+Na]^+$; ^{1}H NMR (500 MHz, $CDCl_3$) δ 4.56–4.47 (m, 4H), 1.48 (*t*, $J=7.1$ Hz, 6H); ^{13}C NMR (125 MHz, $CDCl_3$) δ 154.93, 151.22, 151.01, 150.56, 150.42, 149.19, 149.10, 148.95, 148.56, 148.43, 148.36, 148.32, 147.47, 147.37, 147.15, 146.84, 145.79, 145.76, 144.72, 143.80, 143.70, 143.38, 142.75, 142.69, 142.09, 141.51, 140.65, 136.79, 133.42, 132.66, 130.74, 130.66, 63.31, 14.13; FT-IR (KBr) V_{max} (cm^{-1}) 3846.6, 3743.8, 3424.9, 2916.4, 2357.7, 2318.2, 0.1743.8, 1651.5, 1556.7, 1504.0, 1450.9, 1428.1, 1424.9, 1229.9, 1087.6, 1011.2, 903.2, 855.7, 792.5, 721.3, 673.9, 579.0, 536.9; (Figures S13–S16, Supplementary Material).

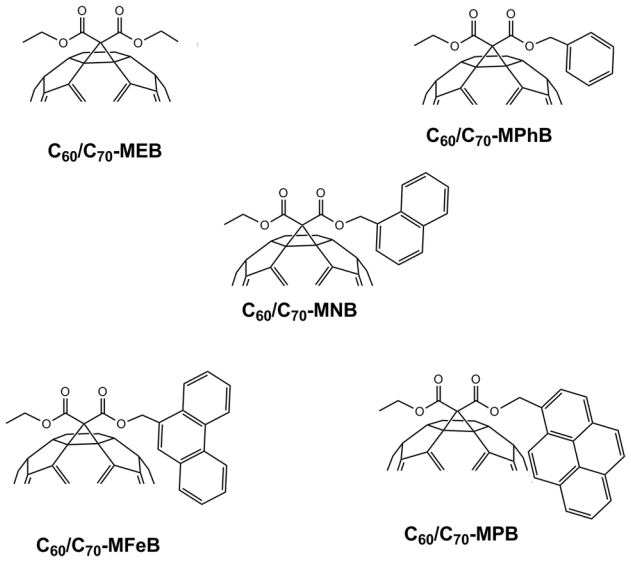

Fig. 2 Structures of synthesized C_{60}/C_{70} fullerene derivatives.

Newly reported C_{60} and C_{70} fullerene derivatives were obtained using modified Bingel synthesis.[23] To a well-stirred solution of C_{60} (144 mg, 0.2 mmol) or C_{70} fullerene (168 mg, 0.2 mmol) dissolved in freshly distilled toluene (110 ml) corresponding to malonate ester (0.2 mmol), a solution of iodine (51 mg, 0.2 mmol) in toluene (10 ml) was added. After 30 min, a solution of DBU (31 µl, 0.2 mmol) in 10 ml of anhydrous toluene was added over a period of 30 min. The obtained mixture was then stirred overnight at room temperature under an argon atmosphere. After concentration using a rotary evaporator, the obtained mixture was chromatographed on silica gel 70–230 using toluene/*n*-hexane 1:1 v/v to yield desired C_{60}/C_{70} fullerene malonates.

61-(Ethyloxycarbonyl)-61-(benzyloxycarbonyl)-1,2-methano[60]fullerene (C_{60}-MPhB) Yield: 36%, ESI–MS 963.9 $[M+Na]^+$;^{1}H NMR (500 MHz, $CDCl_3$) δ 7.52 (dd, $J=8.0$, 1.6 Hz, 2H), 7.44–7.36 (dd, 2H), 5.52 (*s*, 2H), 4.48 (*q*, $J=7.1$ Hz, 2H), 1.36 (*t*, $J=7.1$ Hz, 3H); ^{13}C NMR (125 MHz, $CDCl_3$) δ 163.48, 163.45, 145.26, 145.25, 145.23, 145.21, 145.18, 145.12, 145.09, 144.89, 144.70, 144.68, 144.62, 144.59, 144.57, 143.89, 143.88, 143.07, 143.02, 143.01, 142.98, 142.22, 142.21, 141.92, 141.89, 140.95, 140.93, 139.30, 138.82, 134.66, 129.08, 128.97, 128.73, 68.92, 63.48, 53.44, 14.09; FT-IR (KBr) V_{max} (cm^{-1})

1743.5, 1514.8, 1456.0, 1427.7, 1292.6, 1230.1, 1203.7, 1185.6, 1175.1, 1110.2, 1095.0, 1058.0, 1011.8, 911.6, 738.6, 965.3, 669.3, 596.7, 578.9, 560.9, 551.2, 525.7; (Figures S17–S20, Supplementary Material).

71-(Ethyloxycarbonyl)-71-(benzyloxycarbonyl)-1,2-methano[70]fullerene (C_{70}-MPhB) Yield: 42%, ESI–MS 1084.4 $[M+Na]^+$;^{1}H NMR (500 MHz, $CDCl_3$) δ 7.54–7.26 (m, 2H), 7.26 (m, 2H), 5.47 (s, 1H), 4.50–4.37 (m, 1H), 1.35 (*t*, $J=7.1$ Hz, 2H); ^{13}C NMR (125 MHz, CDCl3) δ 163.34, 163.30, 155.12, 155.01, 151.35, 151.33, 151.32, 151.16, 150.72, 150.69, 150.58, 149.33, 149.25, 149.09, 148.70, 148.67, 148.56, 148.50, 148.47, 147.64, 147.59, 147.52, 147.29, 147.00, 146.45, 145.93, 145.90, 144.92, 144.80, 143.94, 143.83, 143.52, 142.85, 142.81, 142.67, 142.44, 142.05, 141.64, 141.63, 141.00, 140.61, 136.88, 136.76, 134.55, 133.55,, 132.82, 132.80, 130.93, 130.91, 130.90, 130.85, 130.81, 130.80, 129.10, 128.99, 128.75, 68.96, 63.56, 53.44, 14.08; FT-IR (KBr) V_{max} (cm^{-1}) 3440.8, 1743.8, 1556.7, 1419.6, 1361.7, 1216.7, 1082.3, 1016.5, 950.6, 863.6, 792.5, 721.0, 700.3, 573.8, 526.3; (Figures S21–S24, Supplementary Material).

61-(Ethyloxycarbonyl)-61-(naphth-1-ylmethyloxycarbonyl)-1,2-methano[60]fullerene (C_{60}-MNB) Yield: 22%; ESI–MS: 1013.5 $[M+Na]^+$; ^{1}H NMR (500 MHz, $CDCl_3$) δ 8.18–7.49 (m,7H), 5.99 (*s*, 2H), 4.34 (*q*, $J=7.1$ Hz, 2H), 1.21 (*t*, $J=7.1$ Hz, 3H) ppm; ^{13}C NMR (125 MHz, $CDCl_3$) δ 163.57, 163.35, 145.25, 145.23, 145.22, 145.19, 145.15, 145.14, 145.02, 144.94, 144.86, 144.67, 144.64, 144.59, 144.50, 144.45, 143.86, 143.81, 143.03, 142.98, 142.97, 142.93, 142.19, 142.17, 141.82, 141.81, 140.89, 140.83, 139.48, 138.44, 133.82, 131.89, 130.18, 129.11, 128.83, 126.83, 126.19, 125.29, 123.86, 71.60, 67.34, 63.45, 13.92 ppm; FT-IR (KBr) V_{max} (cm^{-1}) 2977.81, 2954.84, 1748.14, 1741.15, 1515.01, 1427.27, 1266.30, 1251.65, 1228.06, 1203.83, 1186.85, 1173.91, 1096.77, 1054.04, 1015.25, 930.53, 799.19, 789.77, 774.62, 727.70, 580.22, 527.06; (Figures S25–S28, Supplementary Material).

71-(Ethyloxycarbonyl)-71-(naphth-1-ylmethyloxycarbonyl)-1,2-methano[70]fullerene (C_{70}-MNB) Yield: 39%; ESI–MS: 1134.4 $[M+Na]^+$; ^{1}H NMR (500 MHz, $CDCl_3$) δ 8.20–7.48 (m, 7H), 5.93 (*s*, 2H), 4.29 (*q*, $J=7.1$ Hz,2H),1.20 (*t*, $J=7.1$ Hz, 3H) ppm; ^{13}C NMR (125 MHz, $CDCl_3$) δ 163.36, 155.13, 154.88, 151.34, 151.27, 151.25, 151.15, 150.68, 150.64, 150.56, 149.29, 149.23, 149.04, 149.01, 148.65, 148.57, 148.50, 148.46, 148.34, 147.54, 147.51, 147.27, 146.99, 146.94, 146.44, 145.89, 145.85, 145.79, 144.92, 144.66, 143.92, 143.81, 143.78, 143.51, 142.83, 142.75, 142.58, 142.48, 141.69, 141.61, 141.47, 141.14, 140.25, 136.89, 136.61, 133.49, 133.45, 132.75, 131.90, 130.87, 130.76, 130.21, 130.14, 129.16, 129.05, 128.86, 128.24, 126.92, 126.23, 125.31, 123.97, 67.40, 63.54, 13.91 ppm; FT-IR (KBr) V_{max} (cm^{-1}) 2946.22, 2911.77, 2851.47, 2359.51, 1740.07, 1700.11, 1652.97, 1558.78, 1539.26, 1506.77, 1456.57, 1428.36, 1268.82, 1249.86, 1234.62, 1225.36, 1161.13, 1131.52, 1093.69, 796.12, 773.69, 726.66, 669.96, 577.75, 533.91; (Figures S29–S32, Supplementary Material);

61-(Ethyloxycarbonyl)-61-(phenanthren-9-ylmethyloxycarbonyl)-1,2-methano[60]fullerene (C_{60}-MFeB) Yield: 41%, ESI–MS: 1040.8 $[M]^-$, ^{1}H NMR (500 MHz, $CDCl_3$) δ 8.73 (*d*, $J=7.7$ Hz, 1H), 8.67 (*d*, $J=8.3$ Hz, 1H), 8.27–8.19 (*m*, 1H), 8.03 (*s*, 1H), 7.94 (d, $J=7.7$ Hz, 1H), 7.88–7.60 (*m*, 5H), 7.26 (*s*, 3H), 6.05 (*s*, 2H), 4.34 (*q*, J=7.1 Hz, 2H), 2.36 (*s*, 1H), 1.55 (*s*, 4H), 1.22 (dd, $J=18.6$, 11.4 Hz, 7H); ^{13}C NMR (126 MHz, $CDCl_3$) δ 163.64, 145.23, 145.21, 145.17, 145.14, 144.98, 144.93, 144.86, 144.67, 144.64, 144.59, 144.39, 143.86, 143.77, 142.97, 142.93, 142.18, 141.82, 141.77, 140.88, 140.83, 139.49, 138.41, 131.07, 131.04, 130.85, 130.41, 129.11, 128.77, 127.65, 127.10, 127.06, 126.92, 124.58, 123.35, 122.63, 67.72, 63.49, 13.95; FT-IR (KBr) ν_{max}(cm^{-1}) 3040.76, 2974.80, 1742.96, 1537.17, 1459.08, 1427.20, 1364.08, 1288.71, 1265.57, 1232.35, 1203.47, 1187.25, 1174.74, 1112.40, 1094.09, 1052.21, 1008.01, 841.51, 755.79, 704.40, 579.99, 554.97, 526.71; (Figures S33–S36, Supplementary Material).

71-(Ethyloxycarbonyl)-71-(phenanthren-9-ylmethyloxycarbonyl)-1,2-methano[70]fullerene (C_{70}-MFeB) Yield: 37%, ESI–MS 1161.4 $[M]^-$; ^{1}H NMR (500 MHz, CDCl3) δ 8.62 (d, $J=8.2$ Hz, 1H), 8.24 (*s*, 1H), 8.01 (*s*, 1H), 7.93 (d, $J=7.9$ Hz, 1H), 7.71–7.62 (*m*, 3H), 7.61 (d, $J=7.0$ Hz, 1H), 5.99 (d, $J=4.2$ Hz, 2H), 4.30 (dd, $J=7.1$, 1.9 Hz, 2H), 2.36 (s, 1H), 1.20 (*t*, $J=7.1$ Hz, 3H). 13C NMR (126 MHz, $CDCl_3$) δ 163.41, 155.13, 154.85, 151.33, 151.25, 151.22, 151.16, 151.14, 150.67, 150.63, 150.58, 150.55, 149.30, 149.28, 149.24, 149.21, 149.03, 148.97, 148.65, 148.50, 148.47, 148.44, 148.21, 147.50, 147.47, 147.27, 147.25, 146.99, 146.92, 146.43, 145.91, 145.89, 145.80, 145.70, 144.93, 144.60, 143.91, 143.80, 143.74, 143.51, 143.47, 142.83, 142.73, 142.61, 142.48, 141.63, 141.60, 141.36, 141.17, 140.11, 136.90, 136.61, 133.48, 133.42, 132.77, 132.65, 131.09, 131.03, 130.91, 130.89, 130.85, 130.78, 130.66, 130.54, 130.39, 129.12, 128.68, 127.66, 127.18, 127.05, 126.95, 124.67, 123.38, 122.62, 67.76, 63.58, 13.95; FT-IR (KBr) ν_{max}(cm^{-1}) 3040.76, 2970.25, 2922.58, 1743.54, 1455.14, 1428.21, 1415.59, 1364.09, 1267.97, 1226.28, 1214.79, 1175.99, 1159.69, 1135.89, 1091.93, 1083.87, 1036.18, 1004.07, 952.86, 841.51, 794.87, 755.37, 725.75, 704.74, 672.71, 577.97, 534.28; (Figures S37-S40, Supplementary Material).

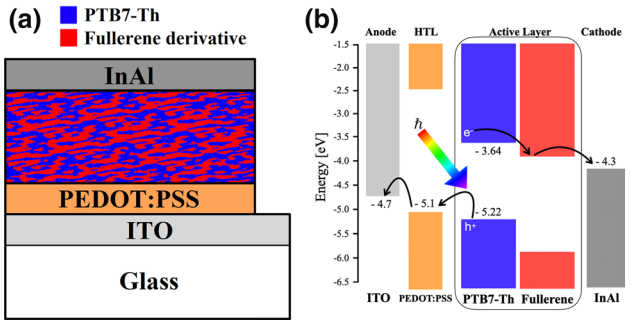

Fig. 3 Standard configuration organic solar cells: (a) layer scheme; (b) energy levels and model of photovoltaic effect.

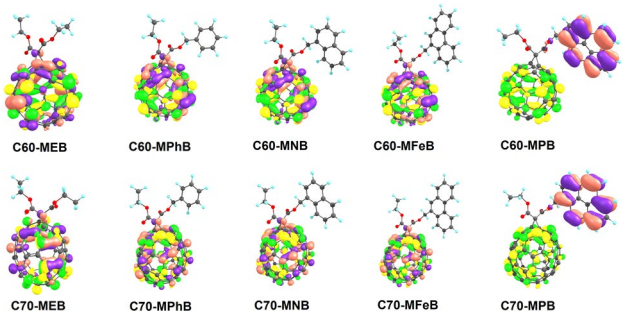

Fig. 4 HOMO (orange and violet) and LUMO (yellow and green) for optimized C_{60} and C_{70} fullerene derivatives. Orange and yellow lobes correspond to positive isosurface values, whereas violet and green lobes to negative isosurface values (Color figure online).

61-(Ethyloxycarbonyl)-61-(pyren-1-yl-methyloxycarbonyl)-1,2-methano[60]fullerene (**C_{60}-MPB**) and 71-(ethyloxycarbonyl)-71-(pyren-1-yl-methyloxycarbonyl)-1,2-methano[70]fullerene (**C_{70}-MPB**) were synthesized as reported previously in the literature.[23,33]

Solar Cell Preparation

Polymer–fullerene bulk heterojunction solar cells of standard architecture were fabricated on the glass substrates covered with indium-tin oxide (ITO).[37]

The structure consisted of a few layers: ITO/PEDOT:PSS/PTB7-Th:fullerene derivative/InAl (see Fig. 3a). The active layer solution contained 97% chlorobenzene (CB) and 3% 1,8-diiodooctane (DIO) as solvent. The total concentration of PTB7-Th:fullerene solution was 20 mg/ml with 2:3 weight ratio. Resulting solutions were stirred for 24 h at 60°C and cooled down to room temperature before deposition. For cell preparation, first, PEDOT:PSS layers of a 40-nm thickness were spin-coated on ITO glass substrate at 5000 rpm for 60 s using an aqueous solution and afterwards annealed at 150°C for 15 min in air. Then the active layer solution was spin-coated in a glovebox under Ar atmosphere at 1500 rpm to a thickness of about 100 nm. The deposited polymer-fullerene bulk heterojunctions (BHJ) were annealed at 80°C for 15 min. Finally, the InAl electrode of 100-nm thickness was deposited by thermal evaporation. We assume that $(InAl)O_3$ spontaneously formed on InAl surface works as a hole-blocking layer. The intersection of ITO and metal electrodes formed eight separate pixels with an area of 4 mm^2 each. The prepared solar cells were encapsulated after first J-V measurements by glass coverslips and epoxy cured under UV light for 15 min. A few 8-pixel cells were prepared for every acceptor.

The scheme of light-induced electronic processes in the heterojunction is presented in Fig. 3b. The photoelectric effect starts from the creation of an electron–hole pair or exciton by a photon. It is followed by diffusion, separation and charge transfer between materials, and finally transferred to electrodes.

Samples for optical absorbance spectroscopy measurements were spin-coated on glass substrates from active layer solutions, or in the case of pure fullerene derivative layers, 20 mg/ml solutions of each compound in CB were prepared and spin-coated at 1000 rpm. For fullerene derivatives that revealed low solubility in CB (C_{60}-MFeB, C_{60}-MPB, C_{70}-MFeB, C_{70}-MPB), 15 mg/ml solutions in carbon disulfide (CS_2) were prepared and spin-coated at 3000 rpm.

Results and Discussion

Quantum Theory Calculations

Electronic distributions of the HOMO and LUMO of investigated C_{60} and C_{70} derivatives are shown in Fig. 4.

Spatial distribution of HOMO and LUMO levels for the optimized structures of almost all investigated fullerene derivatives is similar and covers only the fullerene sphere. The exceptions are pyrene derivatives of C_{60} and C_{70} fullerenes, for which HOMO is located only on the pyrene substituent. Separating the location of HOMO from LUMO and transferring the position of the latter from the fullerene lobe to the pyrene substituent is presumably the cause of its higher energy, which is clear from the comparison of the calculation results for C_{60}-MPB and C_{70}-MPB and, respectively, other C_{60} and C_{70} derivatives (Table I).

Since the reliability of the results obtained with various theoretical approaches depends on the tested systems,[38–40] this paper presents the results obtained with the two most commonly used DFT functionals, B3LYP/6-31G(d) and DFT/PBE/6-311G(d,p), for fullerene derivatives. To theoretically predict electronic properties, more than 400 functionals have already been published; however, two of them, B3LYP and PBE, have now become actually a benchmark.[39]

Table I Computed HOMO/LUMO levels and energy gaps of investigated fullerene derivatives

	Theoretical Frontier Orbital Energy					
	DFT/B3LYP/6-31G(d)			DFT/PBE/6-311G(d,p)		
	HOMO [eV]	LUMO [eV]	*Eg* [eV]	HOMO [eV]	LUMO [eV]	*Eg* [eV]
C60-MEB	−5.67	−3.09	2.58	−5.53	−4.00	1.53
C60-MPhB	−5.69	−3.11	2.58	−5.55	−4.02	1.53
C60-MNB	−5.69	−3.11	2.58	−5.55	−4.02	1.53
C60-MFeB	−5.66	−3.08	2.58	−5.52	−3.99	1.53
C60-MPB	−5.50	−3.10	2.40	−5.22	−4.01	1.22
C70-MEB	−5.61	−3.07	2.54	−5.58	−3.93	1.65
C70-MPhB	−5.60	−3.05	2.55	−5.56	−3.91	1.65
C70-MNB	−5.59	−3.04	2.54	−5.54	−3.90	1.64
C70-MFeB	−5.62	−3.07	2.55	−5.58	−3.94	1.64
C70-MPB	−5.52	−3.08	2.44	−5.25	−3.95	1.30

For the B3LYP functional, a relatively small and inexpensive 6-31G(d) basis set was used because, for compounds containing C, H, N and O, the improvement with increasing basis set size is insignificant. On the other hand, the PBE approach from the 6-311G(d,p) basis set turned out to be very accurate in predicting the energy of HOMO and LUMO for large molecules, including fullerenes and their derivatives.[41] It should be noted that for linear symmetrical/unsymmetrical imines with thiophene and thiazole moieties and for fullerene derivatives C_{60} and C_{70} , the DFT/B3LYP/6-31G(d) approach reflects the experimental HOMO better than the DFT/PBE/6-311G(d,p) method, while the latter method very accurately reflects the energies of LUMO.[22,23] It should be noted that the increase in the energy of HOMO is reflected in the results simulated with both theoretical approaches. The results for LUMO, and consistently for Eg, obtained by both functionals are shifted to each other by approximately 1 eV; however, the trends are the same. This phenomenon has already been discussed before. [16,23,42]

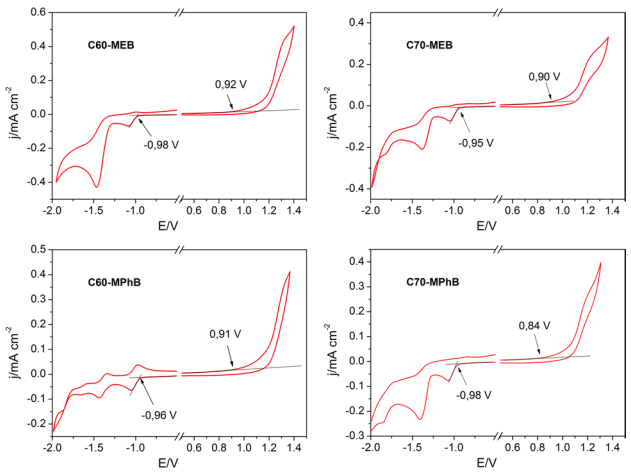

Fig. 5 Cyclic voltammograms obtained on the Pt electrode in DCM solutions containing 0.1 M $TBAPF_6$ and: C_{60}-MEB, C_{70}-MEB, C_{60}-MPhB and C_{70}-MPhB, at the scan rate 0.1 V s^{-1}. The potentials were measured vs. Ag/Ag^+ reference electrode.

Electrochemical Measurements

The exemplary cyclic voltammograms for C_{60}/C_{70}-MEB and C_{60}/C_{70}-MPhB are presented in Fig. 5 (the results obtained for the six other derivatives are shown in Fig. S41, Supplementary Material). Two reversible cathodic peaks visible in each voltammogram relate to the reduction of C_{60} or C_{70} into their anion radicals and dianions,[43] while the irreversible anodic peaks correspond to the oxidation of the substituents attached to the fullerene cages. The reduction and oxidation onset potentials indicated by the arrows, $\boldsymbol{E_{onset}^{red}}$ **and** $\boldsymbol{E_{onset}^{ox}}$, respectively, correspond to the situations when the first electrons were donated or extracted from the fullerenes. Therefore, these values may be used in determination of the LUMO and HOMO energies of the fullerene derivatives. The onset potentials measured vs. Ag/Ag^+ were attributed to the potential of the normal hydrogen electrode (NHE) as described above, and then the LUMO and HOMO energies (in eV) were calculated using the equations

$$E_{\mathrm{LUMO}} = -\left(eE_{\mathrm{onset}}^{\mathrm{red}} + 4.43\ \mathrm{eV}\right) \quad (1)$$

$$E_{\mathrm{HOMO}} = -\left(eE_{\mathrm{onset}}^{\mathrm{ox}} + 4.43\ \mathrm{eV}\right) \quad (2)$$

assuming that 0 V vs. NHE corresponds to 4.43 eV in the absolute scale (versus vacuum).[44]

The obtained values and the band gap energies determined from the difference $\boldsymbol{E_{onset}^{ox} - E_{onset}^{red}}$ (denoted as the electrochemical band gap, $E_{g,EC}$) are listed in Table II.

It is important to note that reduction onset potentials are very similar for all studied derivatives, irrespective of the

Table II Experimental HOMO LUMO levels and energy gaps of investigated fullerene derivatives

	Cyclic voltammetry					Spectral analysis
	E^{ox}_{onset}[V]	E^{red}_{onset}[V]	HOMO [eV]	LUMO [eV]	$E_{g,EC}$ [eV]	E_{opt} [eV]
C60-MEB	0.92	−0.98	−6.02	−4.12	1.90	1.91
C60-MPhB	0.91	−0.96	−6.01	−4.15	1.87	1.91
C60-MNB	0.94	−0.97	−6.04	−4.13	1.91	1.91
C60-MFeB	1.06	−0.89	−6.16	−4.21	1.95	1.91
C60-MPB	0.90	−0.94	−6.00	−4.16	1.84	1.74
C70-MEB	0.90	−0.95	−6.00	−4.16	1.84	1.80
C70-MPhB	0.84	−0.98	−5.94	−4.13	1.82	1.80
C70-MNB	0.87	−0.93	−5.97	−4.17	1.80	1.80
C70-MFeB	0.93	−0.97	−6.03	−4.14	1.90	1.80
C70-MPB	0.88	−0.94	−5.98	−4.16	1.82	1.78

number of rings attached to the malonate group. It was also found that the average value of about -0.96 V vs Ag/Ag^+ is very close to that reported in the literature for C_{60}-MPB.[33]

For comparison, the optical band gaps ($E_{g,opt}$) of all derivatives studied were determined from the onset of absorbance in the UV–vis spectra presented in Fig. 6. The data presented in Table II indicate that the band gap energies obtained from the electrochemical measurements are in a very good agreement with the data determined from absorption spectra, and in general, the band gap values for C_{70} derivatives are slightly lower (by about 0.1 eV) than those for C_{60} analogues. The theoretical energy gaps of the investigated fullerene derivatives differ from the corresponding experimental results. Comparing them to the voltammetric results, they are higher by approximately 0.6 eV for the DFT/B3LYP/6-31G(d) method and lower by approximately 0.4 eV for DFT/PBE/6-311G(d,p), while the greatest contribution to this difference between theory and experiment is the overestimated theoretical value of the energy of the LUMO by approximately 1 eV.

Characterization of Polymer:Fullerene Blends

Figure 7a shows absorbance spectra of pure C_{60} derivatives in solid state. $PC_{60}BM$ and fullerene derivatives bearing 1, 2 or 3 aromatic rings in their structure group (C_{60}-MPhB, C_{60}-MNB and C_{60}-MFeB, respectively) had nearly identical spectra without noticeable differences. The strong absorption is promising for good solar cell performance. The absorbance gradually increases from the 1.2 eV threshold to a maximum at 3.6 eV photon energy.[21,23,45] Absorbance maxima are related to S0-S2 and S0-S3 optical transitions.[46,47] For C_{60}-MPB (four aromatic rings), we observe splitting of the 3.6-eV peak to two with photon energies of 3.5 and 3.7 eV, respectively, similar to the spectra measured for corresponding compound in solution (see Fig. 6). The C_{60}-MEB derivative (without aromatic rings) has the maximum shifted to lower energy by 0.1 eV compared to

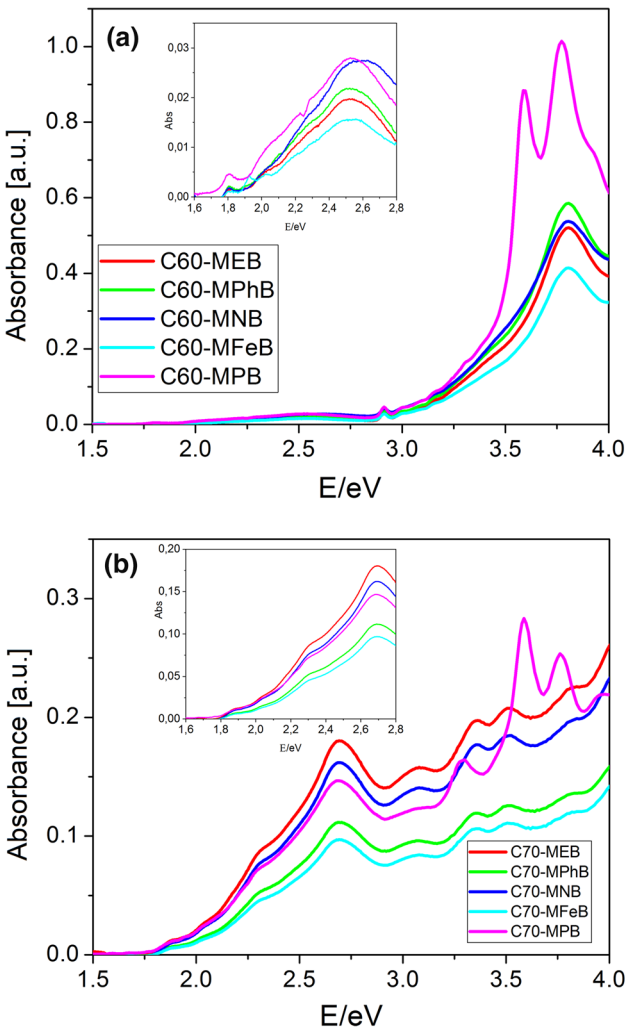

Fig. 6 Absorption spectra of the solutions of C_{60} (a) and C_{70} (b) derivatives in DCM.

$PC_{60}BM$, so it was registered at 3.5 eV. It is noteworthy to mention that in the case of absorbance spectra recorded in solution we can observe a small peak at around 2.9 eV,

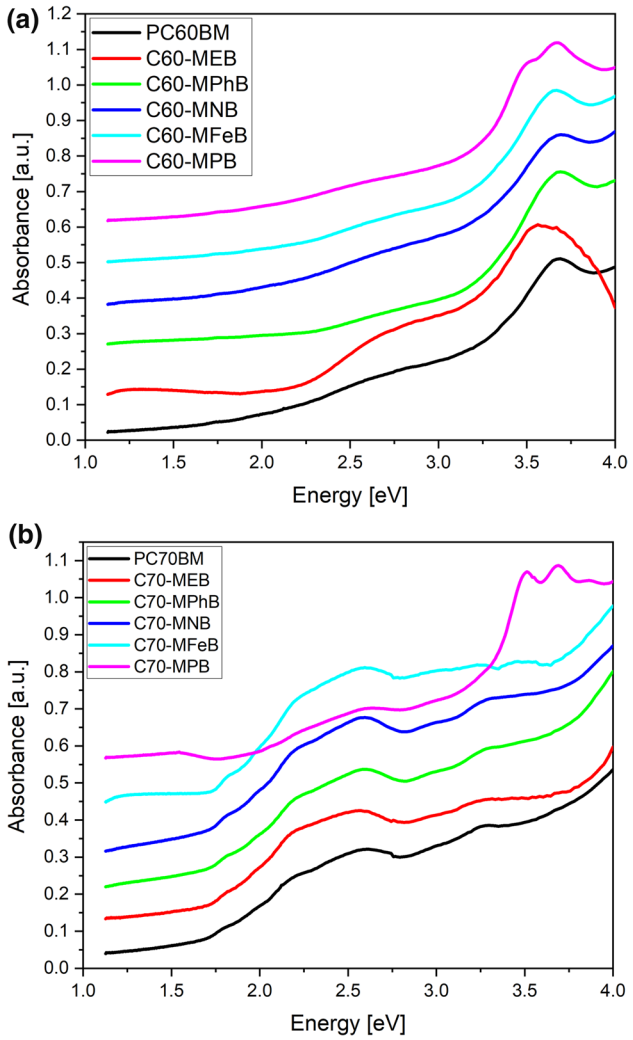

Fig. 7 Optical absorption spectra of fullerene derivative thin films (each subsequent spectrum is vertically shifted by 0.1 for figure clarity): (a) C_{60}, (b) C_{70}.

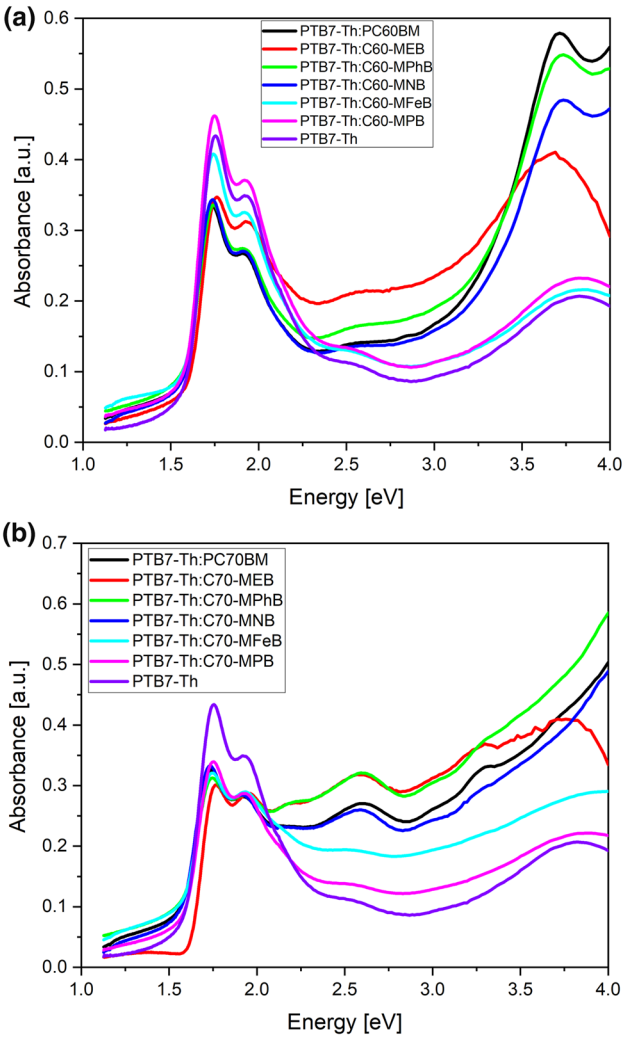

Fig. 8 Optical absorption spectra of thin films of PTB7-Th:fullerenes derivative active layers: (a) C_{60}, (b) C_{70}.

which, as reported previously, can be attributed to the vibrational structure of forbidden electronic transition.[48]

The C_{70} derivatives absorbance spectra (Fig. 7b) showed similar dependence as C_{60} derivatives. The synthesized C_{70} derivatives with 0, 1, 2 and 3 aromatic rings (C_{70}-MEB, C_{70}-MPhB, C_{70}-MNB and C_{70}-MFeB) and commercial $PC_{70}BM$ have identical spectra with a 1.7 eV threshold corresponding to S_0 S_1 transition and broad first maximum at 2.7 eV attributed to S_0T_1 optical transition which is allowed by lower symmetry of the C_{70} molecule.[23,46,49] The 1.7 eV threshold correlates well with the Eg values calculated with DFT/PBE/6-311G(d,p) functional. Additionally, there is a second maximum with small intensity, observed at 3.3 eV. The C_{70} fullerene derivatives are of greater importance in solar cells applications due to their higher absorption in the visible range compared to C_{60} derivatives. For C_{70}-MPB fullerene derivatives, we observed an additional double peak with maxima at 3.5 and 3.7 eV, analogous to the C_{60}-MPB spectrum, which indicates that it is related to pyrene functional group absorption.[23] This could theoretically increase absorption of solar cells in this spectral range. It is consistent with theoretical calculations predicting different LUMO properties for the pyrene derivative (see Fig. 3).

In Fig. 8a and b we present absorption spectra of PTB7-Th:fullerene derivative active layers spin-coated from chlorobenzene. Pure PTB7-Th absorbance starts at 1.6 eV and reaches two maxima at 1.7 eV and 1.9 eV. The peaks are due to transitions from the ground state to the excited one including two different vibrionic states.[50] MPhB, MNB derivatives of both C_{60} and C_{70} MEB are well soluble in chlorobenzene, with an absorption signal comparable to commercial $PC_{60}BM$ and $PC_{70}BM$, while mixtures containing MFeB and MPB showed low signal or even no spectrum characteristic

for fullerenes. This is a result of poor solubility of MFeB and MPB in chlorobenzene, and as a result, the fullerene material was not blended in the layer. Naturally, poorly soluble fullerene derivatives are not suitable as acceptor materials for polymer solar cells, which will be shown further by microscope photos and cell electrical measurements.

Morphology of the active layers analysed by optical microscopy is presented in Fig. 9. The well-soluble derivatives $PC_{70}BM$, C_{70}-MEB, C_{70}-MPhB and C_{70}-MNB (Fig. 9a–d) showed mostly homogeneous polymer:fullerene blend with small visible (~ 10 µm) paths. For the PTB7-Th:C_{70}-MEB layer, we observed a colour change from typical blue to green, which suggested composition variations, for example, polymer:fullerene ratio change.

Photos of blends with PTB7-Th and poorly soluble derivatives C_{70}-MFeB and C_{70}-MPB (Fig. 9e, f), look completely different. The colour is deep green and knowing the absorption spectra can conclude that this layer has low fullerene share blend. There are visible spots size of 10–20 µm that are probably formed by undissolved fullerene derivatives. Comparing pictures for well and poorly soluble materials, it is obvious that the solubility influences also phase separation and structure of the active layer.

As shown in Fig. 3, HOMO in C_{70}-MPB and C_{60}-MPB is highly localized on pyrene moiety. It is well known that localized regions in HOMO are responsible for electron donation during intermolecular interactions, while localized regions in LUMO are acceptance sites. Presumably, the intramolecular π-π stacking interactions[51,52] between extended aromatic electron-rich π systems may even more strongly contribute to the poor solubility of compounds containing conjugated benzene rings and the formation of aggregates as observed by microscope for PTB7-Th:C_{70}-MFeB and PTB7-Th:C_{70}-MPB composites. Similar results were obtained for PTB7-Th:C_{60} layers (they are included in Supplementary Material, Fig. S42).

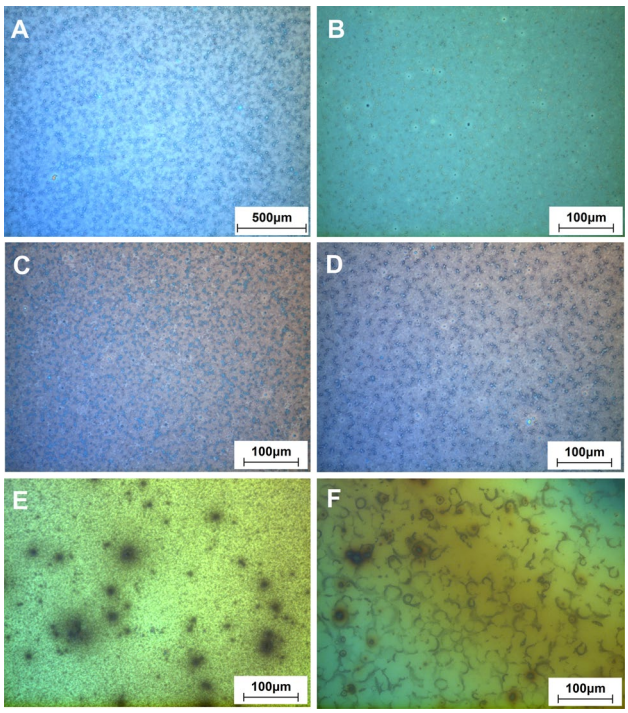

Fig. 9 Morphology of solar cell active layers as observed by microscope with differential interference contrast: (a) PTB7-Th:$PC_{70}BM$, (b) PTB7-Th:C_{70}-MEB, (c) PTB7-Th:C_{70}-MPhB, (d) PTB7-Th:C_{70}-MNB, (e) PTB7-Th:C_{70}-MFeB, (f) PTB7-Th:C_{70}-MPB (Color figure online).

Properties of Solar Cells

Current–voltage (J-V) measurements of solar cells prepared with C_{60} fullerene derivatives (Fig. 10, Table III and Table S1, Supplementary Material) showed very nice J-V characteristics for cells containing MPhB and MNB derivatives. The reference $PC_{60}BM$ cell had a maximum efficiency of 5.3% (8-pixel average 4.9%) and for the $PC_{70}BM$ cell $PCE_{max} = 5.5\%$

The results obtained for different fullerene derivatives generally follow solubility data, so the two best derivatives were C_{60}-MNB and C_{70}-MNB, PCE = 4.0% and 4.1%, respectively. Nearly all cells (except C_{60}-MFeB) had very good conductivity, with series resistance of 6 Ω cm^2 or below. Two well-soluble derivatives C_{60}-MPhB and C_{60}-MNB gave good power conversion efficiencies (PCE) of 3.3% and 4.0%, respectively. The main difference between them and the reference cell was the smaller value of shunt resistance R_{sh}, which caused a decrease of fill factor (FF) and lower short-circuit current (Jsc).

We suppose that the lower Rsh was due to worse quality of the PTB7-Th:fullerene interface that caused reverse

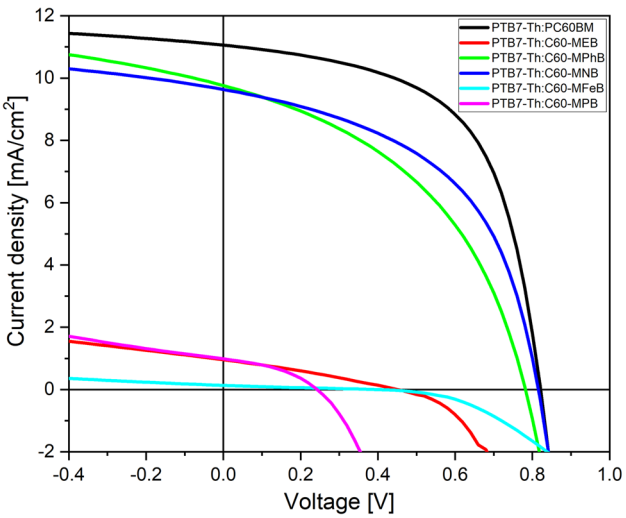

Fig. 10 J-V characteristics of solar cells with PTB7-Th:C_{60} derivative active layers.

Table III Electrical parameters of solar cells with PTB7-Th:C_{60} active layers

Sample	Voc [V]	J_{SC} [mA/cm^2]	R_S [Ω/cm^2]	Rsh [Ω/cm^2]	FF [%]	PCE [%]
$PC_{60}BM$	0.821	11.1	4.46	752	58.6	5.3
C_{60}-MEB	0.453	0.96	4.79	612	28.7	0.12
C_{60}-MPhB	0.782	9.76	5.08	287	43.8	3.3
C_{60}-MNB	0.815	9.63	4.49	433	50.5	4.0
C_{60}-MFeB	0.397	0.13	81.7	2 230	22.5	0.012
C_{60}-MPB	0.243	0.99	6.07	599	39.1	0.09

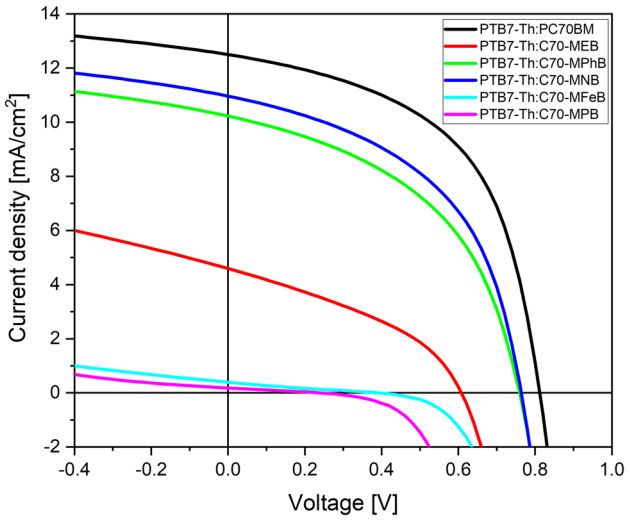

Fig. 11 J-V characteristics of solar cells with PTB7-Th:C_{70} fullerene derivative active layers.

recombination of electrons and holes. However, this can be probably improved by changing the annealing procedure. Open-circuit voltage (Voc) was similar for C_{60}-MNB and the reference $PC_{60}BM$, which confirms good adjustment of HOMO and LUMO levels as shown by quantum mechanical calculation. The poorly soluble C_{60}-MEB and C_{60}-MPB had significantly lower efficiency, a PCE of around 0.1%. The poor C_{60}-MPB performance obviously correlates with a decrease in fullerene content in the blend caused by its low solubility. The lowest efficiency of 0.01% was observed for C_{60}-MFeB, which correlates with the highest content of undissolved fullerene derivatives in PTB7-Th:C_{60}-MFeB blend (Supplementary Material, Fig. S42e). Therefore, we conclude that good solubility is crucial for good performance of the fullerene acceptor material.

Current–voltage measurements together with electrical parameters of solar cells made using C_{70} fullerene derivatives are presented in Fig. 11, Table IV and Table S2 (Supplementary Material). The highest PCE (max 5.5% and av. 4.2%) was obtained for the reference $PC_{70}BM$ derivative. For the five new C_{70} derivatives, the C_{70}-MNB-based cells revealed the highest efficiency, similar to the case of the analogous C_{60} derivatives. It is worth noting that, in general, cells with C_{70} derivatives compared to C_{60} ones had higher Jsc due to greater absorption of the C_{70} derivatives in the visible spectral range.

The two derivatives that revealed good solubility, C_{70}-MPhB and C_{70}-MNB, showed 3.6% and 4.1% efficiency, respectively. They had only slightly lower Voc (by 0.05 V) than the $PC_{70}BM$ cell, which might indicate lower LUMO energy levels of C_{70}-MPhB and C_{70}-MNB. Measured currents were above 10 mA/cm^2 , and similar to the case of C_{60} derivatives, they are also very promising acceptor materials. The lower performance of C_{70}-MFeB and C_{70}-MPB compared to PC70BM was probably caused by the influence of the functional group on polymer:fullerene phase separation inside the blend. The cells with C_{70}-MEB derivative showed minor solubility problems as observed under the optical microscope (Fig. 7b), had a moderate efficiency of 1.1%, mainly due to small Jsc, low Voc and high serial resistance, which suggest poor contact between PTB7-Th and C_{70}-MEB. This weak interaction may be due to the lack of an aromatic ring. The lowest efficiencies, 0.03% and 0.01%, were recorded for both poorly soluble derivatives, C_{70}-MFeB and C_{70}-MPB, with almost two orders of magnitude smaller Jsc then the reference $PC_{70}BM$ cells. Apparently, C_{70}-MFeB and C_{70}-MPB had not incorporated sufficiently inside active layer blend, which resulted in exciton retention in PTB7-Th and stopped charge separation.

Typically, cells with a PTB7-Th:PC70BM active layer have efficiency between 8% and 9%,[53,54] with a recorded PCE of about 11%.[55] Our cells showed lower efficiency at 5.5%; however, they were optimized for repeatability. One of the factors that can affect efficiency is the use of native $(InAl)O_3$ as a hole-blocking layer, which can result in lower efficiency, but in our experiments has given the best repeatability.

The summarizing plot of cell efficiency for different C_{60} and C_{70} derivatives (Fig. 12) was prepared to show dependence on different forms of the investigated fullerene derivatives. The best results were obtained for MNB derivatives that could potentially be applied as a low-cost alternative to commercial C_{60} and C_{70} PCBM derivatives with slightly lower overall efficiency. Also, cells with MPhB fullerenes can be classified as well-functioning, but they

Table IV Electrical parameters of solar cells with PTB7-Th:C_{70} fullerene derivative active layers

Sample	Voc [V]	J_{SC} [mA/cm^2]	R_S [Ω /cm^2]	Rsh [Ω /cm^2]	FF [%]	PCE [%]
$PC_{70}BM$	0.812	12.5	3.96	419	53.8	5.5
C_{70}-MEB	0.608	4.59	9.51	247	37.9	1.06
C_{70}-MPhB	0.760	10.2	4.81	309	46.9	3.7
C_{70}-MNB	0.764	11.0	4.14	330	49.2	4.1
C_{70}-MFeB	0.390	0.39	8.03	777	22.5	0.034
C_{70}-MPB	0.239	0.18	5.84	2 650	26.4	0.011

are characterized by lower electrical parameters and PCE than MNB for both types of fullerenes. Both derivatives have good solubility, so we suppose that the functional group of the fullerene also influences the donor:acceptor phase separation. The MEB derivatives were moderately soluble, and cells with those materials had low PCE, which supports our conclusion that aromatic rings in the functional group of fullerene derivatives improves their mixing in blends with polymer material. Both MFeB and MPB with highest number of aromatic rings in their substituent were poorly soluble in chlorobenzene which resulted in very low efficiencies.

Stability of the Devices

Ageing measurements were carried out for 113 days (16 weeks). During this period, all samples were stored in the dark at room temperature. Normalized PCE was calculated as PCE divided by the first day efficiency (0 days in Fig. 13). T80 was estimated as the time in days for the cell efficiency to drop down to 80% of its initial value.

Figure 13 presents ageing measurements of cells with commercial PCBM and two new fullerene derivatives MNB and MPhB which were characterized by the highest final efficiencies. The cells with PCBM derivatives reveal slightly slower ageing than new derivatives. This PCBM ageing behaviour is typical for cells with standard architecture with PTB7-Th as donor material and PEDOT:PSS as HTL.[56–58] The $PC_{70}BM$ cell is the most stable, with an estimated T80 time of 160–170 days, while the $PC_{60}BM$ cell was slightly worse with the T80 about 130 days. Both C_{60} and C_{70} fullerene derivatives MNB and MPhB age almost the same with T80 time 105 and 115 days, respectively. It can be seen that there is not much difference between the newly synthesized derivatives MNB and MPhB, but there is a visible difference between them and PCBM.

The external quantum efficiency (EQE) spectra were obtained by photocurrent measurements recalculated as a ratio of electron number obtained outside the device (as a current) to the number of incoming photons at each energy (see Fig. 14). The EQE was on the order of 40%, which means that two out of five photons had photoexcited electrons that have reached the cathode. Since the absorbing layers are 100 nm thick, presumably, only half of the photons are absorbed. So we can conclude that nearly all photoexcited electrons reached the cathode.

The cells obtained with MNB and MPhB derivatives were significantly more efficient than the cells prepared with

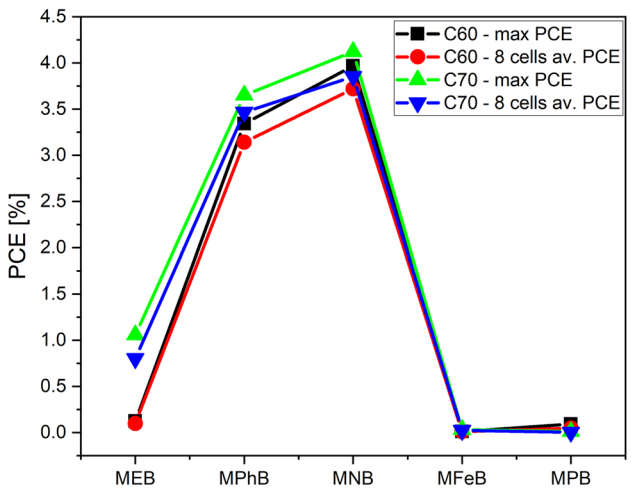

Fig. 12 Maximum and average efficiency PCE for different fullerene derivatives.

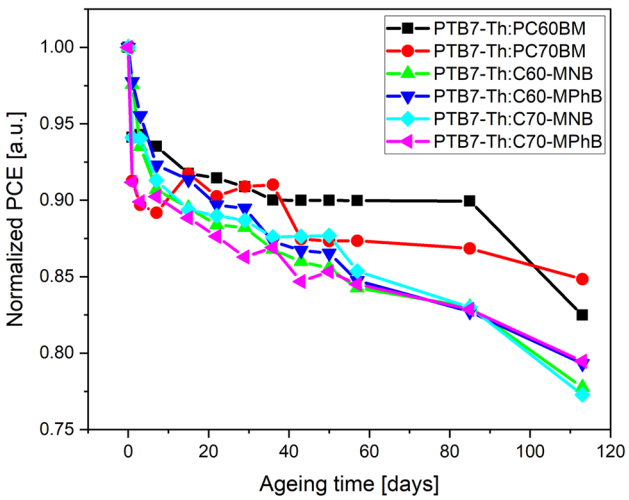

Fig. 13 Ageing of the normalized PCE for encapsulated cells for 113 days in air.

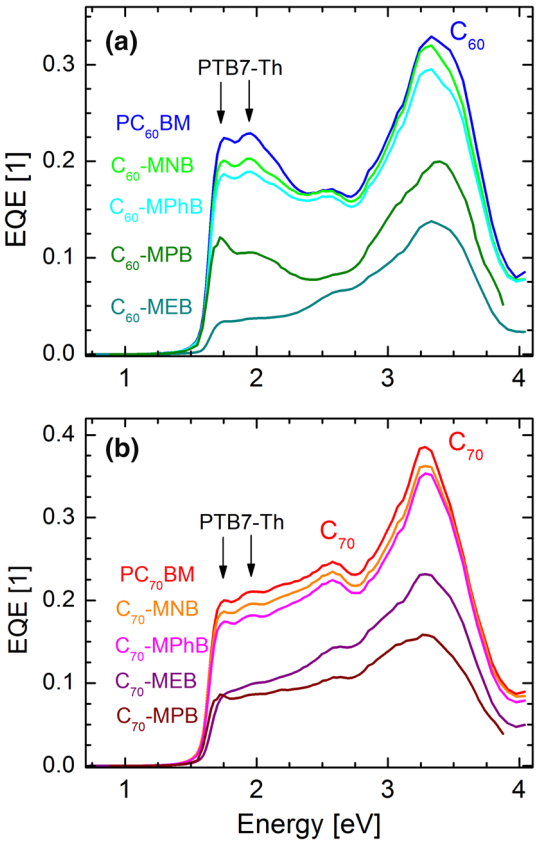

Fig. 14 External quantum efficiency (EQE) spectra of the solar cells with different fullerene derivatives: (a) C_{60} and (b) C_{70} based. Energies of PTB7 absorption peaks are marked by arrows. The characteristic fullerene bands are marked C_{60} and C_{70}.

MEB and MPB, for both C_{60} and C_{70} derivatives. As can be found by comparison of Figs. 8 and 14, absorption peaks of both donor and acceptor materials are visible in the spectra. The 1.76 eV and 1.96 eV peaks of PTB7-Th are marked by arrows.

So the EQE spectra reveal that both materials efficiently absorb photons and that the charge transfer successfully proceeds in both directions. Comparing C_{60} and C_{70} derivative spectra, it can be noticed that C_{70} derivatives have higher absorption in the 2.3–2.8 eV range (in agreement with absorption spectra) which results in higher current generated by cells. The strong decrease of EQE above 3.3 eV is caused by absorption of ITO.

Conclusions

A series of new aromatic C_{60}/C_{70} fullerene derivatives bearing non-aromatic and mono-, bi-, tri- and tetracyclic aromatic substituents were synthesized according to the modified Bingel method, and the resulting compounds were studied as acceptor materials in photovoltaic cells.

It was found that from the synthesized compounds, the MNB C_{70} and C_{60} derivatives allowed us to produce solar cells with the highest efficiency. Moreover, the reported C_{60}/C_{70} MPhB derivatives showed only slightly lower performance. We assign the good performance of MNB and MPhB derivatives to their excellent solubility in chlorobenzene and good mixing with PTB7-Th, which leads to the proper structure of the bulk heterojunction. Long-term ageing measurements showed T80 time between 105 and 115 days for derivatives with mono- and bicyclic aromatic substituents.

The obtained voltage of about 0.8 V allows us to conclude that the HOMO and LUMO levels are well matched to the PTH7-Th ones—they have appropriate offsets. Another factor that increases the efficiency of the reported acceptor materials is their strong optical absorption. The good absorption and efficient separation of charge carriers provided current densities above 10 mA/cm^2. Photocurrent spectroscopy results showed 20–40% quantum efficiency. The energies measured electrochemically and observed in absorption and quantum efficiency spectra were in good agreement with the DFT calculations. Estimation of HOMO energy level was more accurate using the B3LYP/6-31G(d) functional, while calculation of LUMO by the PBE/6-311G(d,p) functional led to values closer to the registered experimental values.

Taking into account that the synthesis of the reported fullerene derivatives is very convenient and easily scalable compared to the most widely used fullerene acceptors, $PC_{60}BM$ and $PC_{70}BM$. While the performance of the obtained photovoltaic devices is satisfactory, the reported compounds are very promising materials for the construction of BHJ solar cells.

Supplementary Information The online version contains supplementary material available at https://doi.org/10.1007/s11664-022-09929-5.

Acknowledgments Authors are grateful for financial support from Polish National Centre of Research and Development (TECHMATSTRATEG 1/347431/14/NCBR/2018). Theoretical calculations were performed by computational resources of the Interdisciplinary Centre for Mathematical and Computational Modelling at Warsaw University (Grant G87-1101).

Conflict of interest There are no conflicts to declare.

References

1. P.K. Nayak, S. Mahesh, H.J. Snaith, and D. Cahen, *Nat. Rev. Mater.* 4, 269 (2019).
2. M. Tao, H. Tamada, T. Druffel, J.-J. Lee, and K. Rajeshwar, ECS. *J. Solid State Sci. Technol.* 9, 125010 (2020).
3. G. Yu, J. Gao, J.C. Hummelen, F. Wudl, and A.J. Heeger, *Science* 270, 1789 (1995).
4. D. Singh, R. Chaudhary, and A. Karthick, *Environ. Sci. Pollut. Res.* 28, 47689 (2021).
5. M.H. Shubbak, *Renew. Sustain. Energy Rev.* 115, 109383 (2019).
6. J. Min, Y.N. Luponosov, C. Cui, B. Kan, H. Chen, X. Wan, Y. Chen, S.A. Ponomarenko, Y. Li, and C.J. Brabec, *Adv. Energy Mater.* 7, 1700465 (2017).
7. R. Ilmi, A. Haque, and M.S. Khan, *Org. Electron.* 58, 53–62 (2018).
8. C. Yan, S. Barlow, Z. Wang, H. Yan, A.K.-Y. Jen, S.R. Marder, and X. Zhan, *Nat. Rev. Mater.* 3, 18003 (2018).
9. R. Ganesamoorthy, G. Sathiyan, and P. Sakthivel, *Sol. Energy Mater. Sol. Cells* 161, 102 (2017).
10. Y. He and Y. Li, *Phys. Chem. Chem. Phys.* 13, 1970 (2011).
11. T. Zheng, H. Zhou, B. Fan, Y. Zhao, B. Jin, L. Fan, and R. Peng, *Chem. Eng. J.* 415, 128816 (2021).
12. W. Huang, E. Gann, N. Chandrasekaran, S.K.K. Prasad, S.-Y. Chang, L. Thomsen, D. Kabra, J.M. Hodgkiss, Y.-B. Cheng, Y. Yang, and C.R. McNeill, *Adv. Energy Mater.* 7, 1602197 (2017).
13. Y. Zhang, A.J. Parnell, O. Błaszczyk, A.J. Musser, I.D.W. Samuel, D.G. Lidzey, and G. Bernardo, *Phys. Chem. Chem. Phys.* 20, 19023 (2018).
14. Y. Matsuo, *Pure Appl. Chem.* 84, 945 (2012).
15. T. Yamanari, T. Taima, J. Sakai, and K. Saito, *Jpn. J. Appl. Phys.* 47, 1230 (2007).
16. J.K. Roy, S. Kar, and J. Leszczyski, *Materials* 12, 2282 (2019).
17. L. Benatto, C.F.N. Marchiori, T. Talka, M. Aramini, N.A.D. Yamamoto, S. Huotari, L.S. Roman, and M. Koehler, *Thin Solid Films* 697, 137827 (2020).
18. L.M. Andersson, Y.-T. Hsu, K. Vandewal, A.B. Sieval, M.R. Anderssson, and O. Inganas, *Org. Electron.* 131, 2856 (2012).
19. F.B. Kooistra, V.D. Mihailetchi, L.M. Popescu, D. Kronholm, P.W.M. Blom, and J.C. Hummelen, *Chem. Mater.* 18, 3068 (2006).
20. H.U. Kim, J.-H. Kim, H. Kang, A.C. Grimsdale, B.J. Kim, S.C. Yoon, D.-H. Hwang, and A.C.S. Appl, *Mater. Interfaces* 6, 20776 (2014).
21. W. Mech, J. Borysiuk, A. Wincukiewicz, R. Bożek, P. Trautman, M. Tokarczyk, M. Kaminska, and K.P. Korona, *Acta Phys. Pol. A* 136, 579 (2019).
22. B. Jewloszewisz, K.A. Bogdanowicz, W. Przybyl, K. Dysz, A. Dylong, A. Gonciarz, R. Pich, W. Mech, K.P. Korona, M. Kaminska, K. Zarębska, M. Skompska, A. Kaim, A. Ciesielski, and A. Iwan, *RSC Adv.* 10, 44958 (2020).
23. P. Piotrowski, W. Mech, K. Zarębska, M. Krajewski, K.P. Korona, M. Kaminska, M. Skompska, and A. Kaim, *Molecules* 26, 1561 (2021).
24. M.B. Upama, M. Wright, B. Puthen-Veettil, N.K. Elumalai, M.A. Mahmud, D. Wang, K.H. Chan, C. Xu, F. Haque, and A. Uddin, *RSC Adv.* 6, 103899 (2016).
25. J. Kettle, Z. Ding, M. Horie, and G.C. Smith, *Org. Electron.* 39, 222 (2016).
26. C.M. Cardona, W. Li, A.E. Kaifer, D. Stockdale, and G.C. Bazan, *Adv. Mater.* 23, 2367 (2011).
27. M.J. Frisch, G.W. Trucks, H.B. Schlegel, G.E. Scuseria, M.A. Robb, J.R. Cheeseman, G. Scalmani, V. Barone, G.A. Petersson, H. Nakatsuji, X. Li, M. Caricato, A.V. Marenich, J. Bloino, B.G. Janesko, R. Gomperts, B. Mennucci, H.P. Hratchian, J.V. Ortiz, A.F. Izmaylov, J.L. Sonnenberg, D. Williams-Young, F. Ding, F. Lipparini, F. Egidi, J. Goings, B. Peng, A. Petrone, T. Henderson, D. Ranasinghe, V.G. Zakrzewski, J. Gao, N. Rega, G. Zheng, W. Liang, M. Hada, M. Ehara, K. Toyota, R. Fukuda, J. Hasegawa, M. Ishida, T. Nakajima, Y. Honda, O. Kitao, H. Nakai, T. Vreven, K. Throssell, J.A. Montgomery, J.E. Peralta, F. Ogliaro, M.J. Bearpark, J.J. Heyd, E.N. Brothers, K.N. Kudin, V.N. Staroverov, T.A. Keith, R. Kobayashi, J. Normand, K. Raghavachari, A.P. Rendell, J.C. Burant, S.S. Iyengar, J. Tomasi, M. Cossi, J.M. Millam, M. Klene, C. Adamo, R. Cammi, J.W. Ochterski, R.L. Martin, K. Morokuma, O. Farkas, J.B. Foresman and D.J. Fox, Gaussian, Inc., Wallingford CT (2016)
28. W. Kohn and L.J. Sham, *Phys. Rev.* 140, A1133 (1965).
29. A.D. Becke, *Phys. Rev.* 38, 3098 (1988).
30. C. Lee, W. Yang, and R.G. Parr, *Phys. Rev. B* 37, 785 (1988).
31. J.P. Perdew, K. Burke, and M. Ernzerhof, *Phys. Rev. Lett.* 77, 3865 (1996).
32. A.L. Gutman and A. Boltanski, *Tetrahedron Lett.* 26, 1573 (1985).
33. M. Ángeles Herranz, C.T. Cox, and L. Echegoyen, *J. Org. Chem.* 68, 5009 (2003).
34. M.D.L. De la Torre, A.C. Tomé, A.M.S. Silva, and J.A.S. Cavaleiro, *Tetrahedron Lett.* 43, 4617 (2002).
35. S. Fujino, M. Yamaji, H. Okamoto, T. Mutai, I. Yoshikawa, H. Houjou, and F. Tani, *Photochem. Photobiol. Sci.* 16, 925 (2017).
36. F. Cheng, X. Yang, H. Zhu, J. Sun, and Y. Liu, *J. Phys. Chem. Solids* 61, 1145 (2000).
37. C. Deibel, and V. Dyakonov, *Rep. Prog. Phys.* 73, 096401 (2010).
38. M. Ernzerhof and G.E. Scuseria, *J. Chem. Phys.* 110, 5029 (1999).
39. P. Borlido, T. Aull, A.W. Huran, F. Tran, M.A.L. Marques, and S. Botti, *J. Chem. Theory Comput.* 15, 5069 (2019).
40. A. Kathiravan, M. Panneerselvam, K. Sundaravel, N. Pavithra, V. Srinivasan, S. Anandand, and M. Jaccob, *Phys. Chem. Chem. Phys.* 18, 13332 (2016).
41. X. Zhang and X.-D. Li, *Chin. Chem. Lett.* 25, 501 (2014).
42. K.A. Bogdanowicz, B. Jewloszewicz, K. Dysz, W. Przybyl, A. Dylong, W. Mech, K.P. Korona, M. Skompska, A. Kaim, M. Kamińska, and A. Iwan, *Electrochim. Acta* 332, 135476 (2020).
43. L. Echegoyen and L.E. Echegoyen, *Acc. Chem. Res.* 31, 593 (1998).
44. H. Reiss and A. Heller, *J. Phys. Chem.* 89, 4207 (1985).
45. O. Ghazy, *Macromol. Symp.* 352, 25 (2015).
46. F. Bencheikh Aboura, D. Duché, J.J. Simon, and L. Escoubas, *Chem. Phys.* 450–451, 102 (2015).
47. M. Ichida, A. Nakamura, H. Shinohara, and Y. Saitoh, *Chem. Phys. Lett.* 289, 579 (1998).
48. H. Ajie, M.M. Alvarez, S.J. Anz, R.D. Beck, F. Diedrich, K. Fostiropoulos, D.R. Huffman, W. Kratschmer, Y. Rubin, K.E. Schriver, D. Sensharma, and R.L. Whetten, *J. Phys. Chem.* 94, 8630 (1990).
49. C.-F. Su, S.-S. Wang, S.-J. Tang, J.-S. Wang, and K.-C. Chiu, *Phys. B Condens. Matter* 405, 3761 (2010).
50. B. Tang, J. Liu, X. Cao, Q. Zhao, X. Yu, S. Zheng, and Y. Han, *RSC Adv.* 7, 17913 (2017).
51. S. Long, W. Chi, L. Miao, Q. Qiao, X. Liu, and Z. Xua, *Chin. Chem. Lett.* 3, 601 (2019).
52. S. Qu, M. Li, L. Xie, X. Huang, J. Yang, N. Wang, and S. Yang, *ACS Nano* 7, 4070 (2013).
53. A.N.M. Alahmadi, *Polymers* 14, 889 (2022).
54. L. Zhang, N. Yi, W. Zhou, Z. Yu, F. Liu, and Y. Chen, *Adv. Sci.* 6, 1900565 (2019).
55. W. Yang, L. Ye, F. Yao, C. Jin, H. Ade, and H. Chen, *Nano Res.* 12, 777 (2019).
56. L. Ciammaruchi, F. Brunetti, and I. Visoly-Fisher, *Sol. Energy* 137, 490 (2016).
57. P. Romero-Gomez, R. Betancur, A. Martinez-Otero, X. Elias, M. Mariano, B. Romero, B. Arredondo, R. Vergaz, and J. Martorell, *Sol. Energy Mater. Sol. Cells* 137, 44 (2015).
58. L. Duan and A. Uddin, *Adv. Sci.* 7, 1903259 (2020).